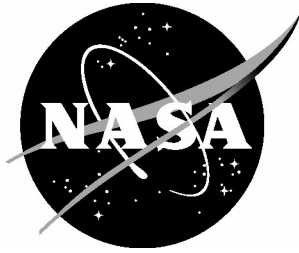# Spectral Characteristics of Wake Vortex Sound During Roll-Up

Yan Zhang and Frank Y. Wang
Volpe National Transportation Systems Center, Cambridge, Massachusetts

Jay C. Hardin
Titan Corporation, Billerica, Massachusetts

December 2003

Since its founding, NASA has been dedicated to the advancement of aeronautics and space science. The NASA Scientific and Technical Information (STI) Program Office plays a key part in helping NASA maintain this important role.

The NASA STI Program Office is operated by Langley Research Center, the lead center for NASA's scientific and technical information. The NASA STI Program Office provides access to the NASA STI Database, the largest collection of aeronautical and space science STI in the world. The Program Office is also NASA's institutional mechanism for disseminating the results of its research and development activities. These results are published by NASA in the NASA STI Report Series, which includes the following report types:

- TECHNICAL PUBLICATION. Reports of completed research or a major significant phase of research that present the results of NASA programs and include extensive data or theoretical analysis. Includes compilations of significant scientific and technical data and information deemed to be of continuing reference value. NASA counterpart of peer-reviewed formal professional papers, but having less stringent limitations on manuscript length and extent of graphic presentations.

- TECHNICAL MEMORANDUM. Scientific and technical findings that are preliminary or of specialized interest, e.g., quick release reports, working papers, and bibliographies that contain minimal annotation. Does not contain extensive analysis.

- CONTRACTOR REPORT. Scientific and technical findings by NASA-sponsored contractors and grantees.

- CONFERENCE PUBLICATION. Collected papers from scientific and technical conferences, symposia, seminars, or other meetings sponsored or co-sponsored by NASA.

- SPECIAL PUBLICATION. Scientific, technical, or historical information from NASA programs, projects, and missions, often concerned with subjects having substantial public interest.

- TECHNICAL TRANSLATION. English-language translations of foreign scientific and technical material pertinent to NASA's mission.

Specialized services that complement the STI Program Office's diverse offerings include creating custom thesauri, building customized databases, organizing and publishing research results ... even providing videos.

For more information about the NASA STI Program Office, see the following:

- Access the NASA STI Program Home Page at *http://www.sti.nasa.gov*

- E-mail your question via the Internet to help@sti.nasa.gov

- Fax your question to the NASA STI Help Desk at (301) 621-0134

- Phone the NASA STI Help Desk at (301) 621-0390

- Write to:
  NASA STI Help Desk
  NASA Center for AeroSpace Information
  7121 Standard Drive
  Hanover, MD 21076-1320

NASA/CR-2003-212673
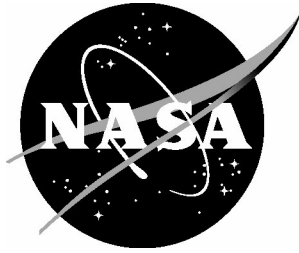
Spectral Characteristics of Wake Vortex Sound During Roll-Up

Yan Zhang and Frank Y. Wang
Volpe National Transportation Systems Center, Cambridge, Massachusetts

Jay C. Hardin
Titan Corporation, Billerica, Massachusetts

December 2003

Available from:

NASA Center for AeroSpace Information (CASI)
7121 Standard Drive
Hanover, MD 21076-1320
(301) 621-0390

National Technical Information Service (NTIS)
5285 Port Royal Road
Springfield, VA 22161-2171
(703) 605-6000

CONTENTS

List of Figures

List of Tables

I. Executive Summary

This report presents an analysis of the sound spectra generated by a trailing aircraft vortex during its rolling-up process. The study demonstrates that a rolling-up vortex could produce low frequency (less than 100 Hz) sound with very high intensity (60 dB above threshold of human hearing) at a distance of 200 ft from the vortex core. The spectrum then drops off rapidly thereafter.

A rigorous analytical approach has been adopted in this report to derive the spectrum of vortex sound. First, the sound pressure was solved from an alternative treatment of the Lighthill's acoustic analogy approach [1]. After the application of Green's function for free space, a tensor analysis was applied to permit the removal of the source term singularity of the wave equation in the far field. Consequently, the sound pressure is expressed in terms of the retarded time that indicates the time history and spacial distribution of the sound source. The Fourier transformation is then applied to the sound pressure to compute its spectrum. As a result, the Fourier transformation greatly simplifies the expression of the vortex sound pressure involving the retarded time, so that the numerical computation is applicable with ease for axisymmetric line vortices during the rolling-up process.

The vortex model assumes that the vortex circulation is proportional to the time and the core radius is a constant. In addition, the velocity profile is assumed to be self-similar along the aircraft flight path, so that a benchmark vortex velocity profile can be devised to obtain a closed form solution, which is then used to validate the numerical calculations for other more realistic vortex profiles for which no closed form solutions are available.

The study suggests that acoustic sensors operating at low frequency band could be profitably deployed for detecting the vortex sound during the rolling-up process.

II.   **Introduction**

The study of aircraft vortices has been a subject of both academic and practical interests for decades [2], [3]. Some of the comparatively matured techniques for characterizing and tracking wake vortices from full scale aircraft have been flow visualization (via wing-tip smoke injection, smoke screen or natural condensation), in-flight probes on penetrating aircraft, instrumented fly-by towers, propeller and sonic anomometer arrays, acoustic radars, LDV/CW-Lidar and pulsed-Lidars [4]–[15]. Exploratory efforts have also been made in the areas of, for examples, RASS, Radar, pressure transducer array, infrared sensing, microwave radiometry and passive acoustics [3], [4], [16]–[20]. The present report examines the acoustic emission of aircraft vortices, in response to the renewed interest in studying the passive wake acoustic detection scheme.

A number of field observations have indicated that vortices emit audible sound when in the near proximity of the ground. Frequencies from 1 to 5 KHz have been reported [4], and various descriptions of the wake sound have been described from "whooshing", "whine", "crackling" to "roaring" [4], [7]. During early days of wake vortex sensor research, the aforementioned acoustic emission phenomenon was not deemed reliable enough as the basis of a sensor for tracking wakes near the ground. Consequently, no effort had been devoted over the years to systematically study the acoustic emission from aircraft wakes. More recently, unpublished measurements of exploratory nature from NOAA [21] indicated that vortices also emit infrasound. The general area of aircraft wake acoustics however, unlike other branches of aeroacoustics involving jets, airframe and blade-vortex interaction, has not received the comparable level of attention over the course of noise research. Consequently, fundamental issues such as the spectral characterization, its associated uniqueness and consistency, as well as over what frequency band could wake vortices be tracked effectively and practically, still remain to be addressed. In response to the renewed interest in tracking and characterizing wakes with a passive acoustics approach, the present report represents a first step in analytically examining the spectral characteristics of aircraft vortices during its initial generation phase at altitude.

The analytical study of sound generation aerodynamically has been a continuing research area since the acoustic analogy approach pioneered by Lighthill [1]. Representa-

tive studies that have since been influenced by Lighthill, examined the acoustic signature stemming from stretching or spinning vortex rings [22], and by ring vortices interacting with structure [23] or with other vortex rings [24]. In these studies, the vortex velocity was treated as a source and the vortex pressure was evaluated by integrating the product of the time-retarded Green's function and the source term over the entire region of vortex velocity distribution [23], [25]. The time-retarded Green's function was expanded in terms of its retarded time in the far field, so that the vortex pressure was expressed in the form of a Taylor series and evaluated by truncating higher order terms. In studying the sound generated by aircraft wakes, the present report adopted a tensor analysis instead, to simplify the "source" term in the acoustic analogy approach. The spectrum of vortex pressure is expressed as the trace of the integration of a matrix. The study then examines the acoustic spectrum of a straight line vortex at altitude developing over a microphone array. A closed form solution of the spectrum of the vortex pressure field is obtained for a benchmark vortex profile, and is used for validation of the numerical method for other profiles where closed form solutions are not available. The development of the analysis is presented as follows.

III. Formulation of the Governing Equation

A. *Vortex Sound Wave Equation*

The sound pressure, p, of an inviscid flow field is governed by the following set of equations [23]

$$\frac{\partial}{\partial t}\rho + \nabla \cdot (\rho\bar{u}) = 0 \tag{1}$$

$$\frac{\partial}{\partial t}(\rho\bar{u}) + \nabla \cdot (\rho\bar{u}\,\bar{u}) + \nabla p = 0 \tag{2}$$

$$dp = c_o^2 d\rho \tag{3}$$

where c_o is the sound speed, ρ is density, p is pressure, and $\bar{u}$ is velocity field. Following the arguments of Kambe [23] for an incompressible flow, i.e., $\rho = \rho_o$ the equations of motion are reduced to a wave equation involving pressure, classically known as the Lighthill's acoustic analog equation [1]:

$$\nabla^2 p - \frac{1}{c_o^2}\frac{\partial^2}{\partial t^2}p = -\rho_o\nabla \cdot [\nabla \cdot (\bar{u}\bar{u})] \tag{4}$$

The right hand side of (4) may then be interpreted as a "source" term for generating the pressure p. Far away from a source where the velocity $\bar{u}$ is zero or a constant, Eq. (4) is then satisfied by a spherical wave solution.

B.   Solution of Vortex Sound Pressure

The solution of the vortex sound pressure from the wave equation (4) can be expressed as an integration involving the Green's function as [26]

$$p(\bar{r}, t) = -\rho_o \iint g(\bar{r} - \bar{r}'; t - t') \left\{ \nabla' \cdot \nabla' \cdot [\bar{u}(\bar{r}', t')\bar{u}(\bar{r}', t')] \right\} d\bar{r}' dt' \tag{5}$$

where g is the time-retarded Green's function in free space

$$g(\bar{r} - \bar{r}'; t - t') = \begin{cases} 0 & \text{if } t < t' \\ -\dfrac{c_o}{4\pi |\bar{r} - \bar{r}'|} \delta\left[|\bar{r} - \bar{r}'| - c_o(t - t') \right] & \text{if } t > t' \end{cases} \tag{6}$$

with δ representing the delta function. By applying the identities described in Eqs. (49) and (51) in Appendix A, and using the divergence theorem where the surface integral terms are ignored, one obtains

$$p(\bar{r}, t) = -\rho_o \text{trace} \iint \left(\bar{u}(\bar{r}', t')\bar{u}(\bar{r}', t') \right) \cdot \nabla' \nabla' g \left(\bar{r} - \bar{r}'; t - t' \right) d\bar{r}' dt' \tag{7}$$

The expression with the index notation is then obtained as

$$p(\bar{r}, t) = -\rho_o \iint \left(u_j(\bar{r}', t')u_i(\bar{r}', t') \right) \frac{\partial}{\partial x_i'} \frac{\partial}{\partial x_j'} g \left(\bar{r} - \bar{r}'; t - t' \right) d\bar{r}' dt' \tag{8}$$

Note that the relation of

$$\frac{\partial}{\partial x_i'} \frac{\partial}{\partial x_j'} = \frac{\partial}{\partial x_i} \frac{\partial}{\partial x_j} \tag{9}$$

holds for the Green's function, then Eq. (8) becomes

$$p(\bar{r}, t) = -\rho_o \frac{\partial}{\partial x_i} \frac{\partial}{\partial x_j} \iint \left(u_i(\bar{r}', t')u_j(\bar{r}', t') \right) g \left(\bar{r} - \bar{r}'; t - t' \right) d\bar{r}' dt' \tag{10}$$

Placing the Green's function into Eq. (10) yields

$$p(\bar{r}, t) = c_o \rho_o \frac{\partial}{\partial x_i} \frac{\partial}{\partial x_j} \iint \left(u_i(\bar{r}', t')u_j(\bar{r}', t') \right) \frac{\delta\left[|\bar{r} - \bar{r}'| - c_o(t - t') \right]}{4\pi |\bar{r} - \bar{r}'|} d\bar{r}' dt' \tag{11}$$

Furthermore, by performing the integration over t', one obtains

$$p(\bar{r}, t) = \rho_o \frac{\partial}{\partial x_i} \frac{\partial}{\partial x_j} \int \frac{1}{4\pi |\bar{r} - \bar{r}'|} u_i \left(\bar{r}', t - \frac{|\bar{r} - \bar{r}'|}{c_o} \right) u_j \left(\bar{r}', t - \frac{|\bar{r} - \bar{r}'|}{c_o} \right) d\bar{r}' \tag{12}$$

Applying the property

$$\frac{\partial}{\partial x_i} = -\frac{x_i - x_i'}{|\bar{r} - \bar{r}'| c_o} \frac{\partial}{\partial t} \tag{13}$$

in the far field where $|\bar{r} - \bar{r}'| \approx r$ and $(x_i - x_i') \approx x_i$, Eq. (12) is then approximated as

$$p(\bar{r}, t) \approx \frac{\rho_o}{4\pi r c_o^2} \frac{x_i x_j}{r^2} \frac{\partial^2}{\partial t^2} \int u_i \left(\bar{r}', t - \frac{|\bar{r} - \bar{r}'|}{c_o}\right) u_j \left(\bar{r}', t - \frac{|\bar{r} - \bar{r}'|}{c_o}\right) d\bar{r}' \tag{14}$$

Note that Eq. (14) is identical to the expression provided by Powell in Ref. [27].

C.   Remarks on Retarded Time

The retarded time, $t - |\bar{r} - \bar{r}'|/c_o$, that appears in Eq. (14) where c_o is the speed of sound, is introduced by the retarded-time Green's function (6). It describes the time history of the vortex sound sources. In the far-field, where $|\bar{r} - \bar{r}'| \approx r - (\bar{r}/r) \cdot \bar{r}'$, the retarded time is approximated as

$$t - \frac{|\bar{r} - \bar{r}'|}{c_o} \approx \left(t - \frac{r}{c_o}\right) + \frac{\bar{r}}{c_o r} \cdot \bar{r}' \tag{15}$$

Note that the last term on the right-hand side of the above equation is the function of the orientation for the source position $(\bar{r}')$ with respect to the direction of observation $(\bar{r}/r)$, and it does not depend on the distance to the observer (since $\bar{r}/r$ is a unit vector). Thus this term should ideally be kept when carrying out the integration over r' as performed in Eq. (14), which formed the basis of subsequent development.

IV.   Formulation of Vortex Sound Spectrum

In obtaining the spectrum of a vortex sound pressure, the Fourier transformation can be applied directly to Eq. (5) without performing complicated mathematical manipulations from Eq. (7) to Eq. (14). Denoting the term in the integrand as

$$f(\bar{r}', t') = \nabla' \cdot [\nabla' \cdot \bar{u}(\bar{r}', t') \bar{u}(\bar{r}', t')] \tag{16}$$

and utilizing the selection property of the delta (δ) function, a more compact form for Eq. (5) is then obtained,

$$p(\bar{r}, t) = \rho_o \int \frac{1}{4\pi |\bar{r} - \bar{r}'|} f\left(\bar{r}', t - \frac{|\bar{r} - \bar{r}'|}{c_o}\right) d\bar{r}' \tag{17}$$

Note that Eq. (17) represents a general solution of vortex pressure field governed by Eq. (4) for an arbitrary profile of velocity distribution. Theoretically, knowing the velocity profile $\bar{u}$, the pressure can be evaluated directly, although the calculation involving double gradients on the velocity field may be sensitive to errors introduced by numerical procedure. Next, to obtain the spectrum of the vortex sound, Fourier transformation is applied directly on the integral representation of the pressure, and then an alternative form is obtained by operating the double gradients on the scalar Green's function, instead of the vortex velocity field.

A. Fourier Spectrum of Vortex Sound Pressure

The spectral character of vortex sound is obtained by the Fourier transformation of

$$P(\bar{r}, \omega) = \iint \frac{\rho_o}{4\pi \left|\bar{r} - \bar{r}'\right|} f\left(\bar{r}', t - \frac{\left|\bar{r} - \bar{r}'\right|}{c_o}\right) e^{j\omega t} d\bar{r}' dt \tag{18}$$

where ω is angular frequency. By writing the retarded time as $t' = t - |\bar{r} - \bar{r}'|/c_o$, Eq. (18) becomes

$$P(\bar{r}, \omega) = \rho_o \int \frac{e^{j\omega|\bar{r} - \bar{r}'|/c_o}}{4\pi \left|\bar{r} - \bar{r}'\right|} F(\bar{r}', \omega) d\bar{r}' \tag{19}$$

where $F(\bar{r}', \omega)$ is the Fourier transform of $f(\bar{r}', t')$. In addition, defining the tensor

$$\overline{\overline{A}}(\bar{r}', \omega) = \int \left[\bar{u}(\bar{r}', t')\bar{u}(\bar{r}', t')\right] e^{j\omega t'} dt' \tag{20}$$

and writing the scalar Green's function as

$$\phi(\bar{r}, \bar{r}') = \frac{e^{j\omega|\bar{r} - \bar{r}'|/c_o}}{4\pi \left|\bar{r} - \bar{r}'\right|} \tag{21}$$

Eq. (19) is simplified as

$$P(\bar{r}, \omega) = \rho_o \operatorname{trace} \int \left(\overline{\overline{A}}(\bar{r}', \omega) \cdot \nabla'\nabla'\phi(\bar{r}, \bar{r}')\right) d\bar{r}' \tag{22}$$

The details of the derivation are found in Appendix A. The *trace* operator is the summation of diagonal elements in the matrix representation of a tensor. Given the vortex velocity profile $\bar{u}$, the tensor $\overline{\overline{A}}$ can be calculated from Eq. (20). In addition, $\nabla'\nabla'\phi$ can be computed using the definition of ϕ in Eq. (21). Finally, the spectrum of vortex sound pressure expressed in Eq. (22) can be evaluated quantitatively. Note that the evaluation of the spectrum involves integrations over time t' (20) as well as local space $\bar{r}'$ (22).
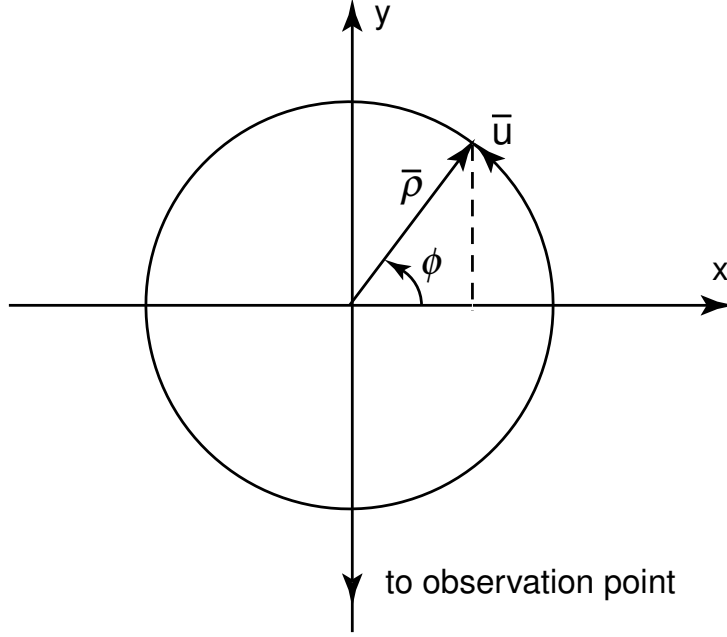
Fig. 1. Nomenclatures for the axisymmetric trailing vortex.

B.   Far-Field Representation of Vortex Sound Spectrum

For practical reasons, far-field approximation of the pressure spectrum for vortex sound is of particular interest. In the far field, where $r \gg r'$ and $|\bar{r} - \bar{r}'| \approx r - \bar{r} \cdot \bar{r}'/r$, the term $\nabla'\nabla'\phi$ in the integrand of Eq. (22) becomes, by keeping the lowest-order term with respect to $1/|\bar{r} - \bar{r}'|$,

$$\nabla'\nabla'\phi \approx -\bar{r}\bar{r}\,\frac{\omega^2\,e^{j\omega|\bar{r}-\bar{r}'|/c_o}}{c_o^2\,\pi\,r^3} \tag{23}$$

Therefore the spectrum in the far field can be expressed approximately as

$$P(\bar{r},\omega) \approx -\mathrm{trace}\left\{\frac{\omega^2\rho_o}{c_o^2\pi r}e^{j\omega r/c_o}\int \overline{\overline{A}}(\bar{r}',\omega)\cdot\frac{\bar{r}\bar{r}}{r^2}\,e^{-j\frac{\omega}{c_o}\hat{r}\cdot\bar{r}'}d\bar{r}'\right\} \tag{24}$$

where ω^2 is due to the double-gradient operation of the scalar Green's function. Note that the spectrum strength is inversely proportional to the distance r by knowing that $(\bar{r} - \bar{r}')\,(\bar{r} - \bar{r}')/r^2$ approaches to a unit tensor for large r. Also note that, at $\omega = 0$, the pressure spectrum is zero, i.e., $P(\bar{r},\omega = 0) = 0$, which confirms that vortex sound does not contain a DC component.

Given the velocity profile, the general form of spectrum for vortex sound in the far field, Eq. (24), can be evaluated numerically. Axisymmetry of the vortex velocity is assumed

for the analysis, whose nomenclatures is illustrated in Fig. (1). The axisymmetric line vortex field in space and time is also assumed to have the following general form,

$$\bar{u}\left(\bar{r}', t'\right) = \hat{\phi}' \left[S\left(z' - L_1\right) - S\left(z' - L_2\right)\right] \Phi\left(\rho', t'\right) \tag{25}$$

where $\hat{\phi}'$ is a unit vector in the circumferential direction, and S is the step function defined as

$$S(z) = \begin{cases} 0 & z < 0 \\ 1 & z \geq 0 \end{cases} \tag{26}$$

and $\Phi(\rho', t')$ is the scalar velocity field.

V.   Rolling-Up Vortices with Constant Longitudinal Distribution

The vortex during the rolling-up process is assumed to be longitudinally constant, so that the variables ρ' and t' are separable and the velocity is re-written as

$$\bar{u}\left(\bar{r}', t'\right) = \hat{\phi}' \left[S\left(z' - L_1\right) - S\left(z' - L_2\right)\right] \Phi\left(\rho'\right) f(t') \tag{27}$$

where $f(r')$ is the ramping function defined as

$$f(t') = \begin{cases} 0 & t' \leq -T \\ \left(t' + T\right)/T & -T < t' \leq 0 \\ 1 & t' > 0 \end{cases} \tag{28}$$

with T denoting the time constant, and $\Phi(\rho')$ representing the velocity profile in cylindrical coordinates. Eq. (27) shows that the velocity distribution along the flight path (z-axis) is constant in the region of $L_1 < z < L_2$. Also notice that the time constant T is approximately the rolling-up time of a vortex. The rolling-up distance for an elliptically loaded clean wing is at least between 2-3 aircraft spans downstream [28], thus on an average,

$$T \approx 2.5 \frac{s}{U} \tag{29}$$

where s is aircraft wing span, and U is the landing approach speed.

With the definition of the ramping function $f(t')$ in Eq. (28), the tensor, defined in Eq. (20), then becomes

$$\begin{aligned} \overline{\overline{A}}(\bar{r}', \omega) &= \hat{\phi}' \hat{\phi}' \, \Phi^2(\rho') \left[S\left(z' - L_1\right) - S\left(z' - L_2\right)\right] \\ &\quad \cdot \frac{2}{T\omega^2} \left[1 - \frac{1}{jT\omega}\left(1 - e^{-j\omega T}\right)\right] \end{aligned} \tag{30}$$

Eq. (30) shows that tensor $\overline{\overline{A}}$ is an even function of the velocity profile, $\Phi(\rho')$, therefore another vortex of the opposite sign will generate the same sound pressure, except an extra consideration of the distance to the observation point. Note that Eq. (27) represents a line vortex that is rolling up into a fully developed vortex in a longitudinal region bounded by $L_1 < z < L_2$ during time T, where $L_2 - L_1$ is determined by the coverage area of an array of acoustic wave sensors. Also note that the line vortex situated in a finite layer, so that the vortex field is localized and the radiation condition [29] is satisfied in the formulation. The assumption reflects the physical situation that local vortex sound is sampled by using a directional acoustic sensor, such as a phased microphone array as discussed in Sec. V-D.

Upon introducing $\overline{\overline{A}}$ in Eq. (30) into Eq. (24), the spectrum is found as

$$
\begin{aligned}
P(\bar{r}, \omega) &= \text{trace}\Big\{ B(\omega) \frac{\rho_o}{c_o^2 \pi r} e^{j\omega r/c_o} \int \hat{\phi}' \hat{\phi}' \cdot \hat{r}\hat{r} \, \Phi^2(\rho') \\
&\quad \cdot \left[S(z' - L_1) - S(z' - L_2) \right] e^{-j\omega \hat{r} \cdot \bar{r}'/c_o} d\bar{r}' \Big\}
\end{aligned}
\tag{31}
$$

where

$$
B(\omega) = \frac{2}{T} \left[\frac{1}{jT\omega} \left(1 - e^{-j\omega T} \right) - 1 \right]
$$

Furthermore, given the position of observation point $\bar{r} = -r\hat{y}$ as shown in Fig. (1), and denoting $\bar{r}' = \hat{x}\rho' \cos\phi' + \hat{y}\rho' \sin\phi' + \hat{z}z'$ and $\hat{\phi}' = -\hat{x}\sin\phi' + \hat{y}\cos\phi'$, Eq. (31) is then obtained as

$$
\begin{aligned}
P(\bar{r}, \omega) &= B(\omega) \frac{\rho_o}{c_o^2 \pi r} (L_2 - L_1) e^{j\omega r/c_o} \\
&\quad \cdot \int \cos^2\phi' \, \Phi^2(\rho') e^{j\frac{\omega}{c_o}\rho' \sin\phi'} \rho' d\rho' d\phi'
\end{aligned}
\tag{32}
$$

Noticing that the integration with respect to the angle ϕ gives

$$
\int \cos^2\phi' \, e^{j\frac{\omega}{c_o}\rho' \sin\phi'} d\phi' = \pi \left[J_0\left(\omega\rho'/c_o\right) + J_2\left(\omega\rho'/c_o\right) \right]
\tag{33}
$$

where J_0 and J_2 are the zeroth and second order Bessel functions of the first kind, respectively. In addition, by using the recursive formula [30]

$$
J_{n-1}(z) + J_{n+1}(z) = \frac{2n}{z} J_n(z)
\tag{34}
$$

Eq. (32) is furthermore simplified as

$$
P(\bar{r}, \omega) = B(\omega) \frac{2\rho_o}{c_o \omega r} (L_2 - L_1) e^{j\omega r/c_o} \int_0^\infty \Phi^2(\rho') J_1(\omega\rho'/c_o) d\rho'
\tag{35}
$$

The above integration involves a single-fold integration in terms of radial distance ρ', therefore the computation is more efficient than the multiple-fold integration of the previous expression.

A. Example Vortex Profiles

The two vortex profile models considered in this report are the Hallock-Burnham vortex [3] and the Lamb-Ossen vortex [3]. Both profile models are axisymmetric, with the former expressed as

$$\Phi(\rho') = \frac{\Gamma_o}{2\pi\rho'} \frac{\rho'^2}{\rho'^2 + \rho_c^2} \tag{36}$$

where Γ_o is the circulation and ρ_c is the vortex core radius, and the latter defined as

$$\Phi(\rho') = \frac{\Gamma_o}{2\pi\rho'} \left\{ 1 - \exp\left[-1.2526 \left(\frac{\rho'}{\rho_c} \right)^2 \right] \right\} \tag{37}$$

The core radius, ρ_c, defined as the distance between the locations of zero tangential velocity to where the maximum value occurs, is the same for both of the vortex profile models. However the peak values are different, e.g.,

$$\frac{\Gamma_o}{4\pi\rho_c}$$

for the Hallock-Burnham vortex and

$$\frac{\Gamma_o}{2\pi\rho_c} \left(1 - e^{-1.2526} \right)$$

for the Lamb-Oseen vortex. For both of the vortex profile models selected, closed form solutions of the sound spectra are not achievable. The acoustic spectra of these vortex profile models are therefore obtained via numerical integration of Eq. (35).

B. Validation Using Benchmark Vortex Profile

For the purpose of validating the numerical integration program, a benchmark vortex velocity profile which allows a closed form solution to Eq. (35) is prescribed as

$$\Phi(\rho') = \frac{\Gamma_o}{4\pi\rho_c^2} \rho' e^{1 - \frac{\rho'}{\rho_c}} \tag{38}$$

with the core radius, ρ_c, and the peak value, $\Gamma_o/(4\pi\rho_c)$, being the same as the Hallock-Burnham vortex, but with a faster decay for $\rho > \rho_c$. With this definition of the vortex

profile, a closed form formula of the spectrum of sound pressure, with the derivation shown in detail in Appendix B, is obtained as

$$P(\bar{r}, \omega) = \frac{3\rho_o e^2}{2c_o^2 \rho_c^4 \pi r} \left(\frac{\Gamma_o}{2\pi}\right)^2 (L_2 - L_1) e^{j\omega r/c_o} A(\omega) B(\omega) \tag{39}$$

where

$$
\begin{aligned}
A(\omega) &= \frac{\pi}{(a^2 + b^2)^2} \left(5\alpha_o^2 + 1\right) \\
&+ \frac{2a\pi}{\left(\sqrt{a^2 + b^2}\right)^5} \alpha_o \left(5\alpha_o^2 + 3\right) \\
&+ \frac{5a^2\pi}{4(a^2 + b^2)^3} \left(\alpha_o^2 + 1\right) \left(5\alpha_o^2 + 1\right) \\
&+ \frac{5a^3\pi}{4\left(\sqrt{a^2 + b^2}\right)^7} \alpha_o \left(\alpha_o^2 + 1\right)^2
\end{aligned}
\tag{40}
$$

and

$$\alpha_o = \frac{2c_o}{\rho_c \omega} \left[1 - \sqrt{1 + \left(\frac{\rho_c \omega}{2c_o}\right)^2}\right] \tag{41}$$

$$a = \omega/c_o \tag{42}$$

$$b = 2/\rho_c \tag{43}$$

It demonstrates that the vortex sound is independent on the sign of circulation, Γ_o. Also notice that the spectrum of the vortex pressure is roughly proportional to Γ_o^2 and inversely proportional to ρ_c^4 at high frequency. This implies that, taking into account that Γ_o/ρ_c is roughly a constant for current civil transport aircraft, a vortex with a large core (usually produced by larger aircraft), generates weaker sound in the high frequency regime.

C.   Numerical Results and Discussions

The numerical evaluation of the spectrum expressed in Eq. (35) is then applied to a line vortex with the two commonly employed profile models indicated in Eqs. (36) and (37). As indicated earlier, a numerical code was developed to carry out the integration in Eq. (39), and the vortex profile of Eq. (38) was devised in order to provide a closed form solution for the purpose of validating the computer program. Characteristics of B747

TABLE I

CONSTANT PARAMETERS FOR VARIOUS AIRCRAFT

	Circulation $[\text{m}^2/s]$	Wing Span [m]	Landing Speed [m/s]
B747	600	60	66
B757	360	38	66

TABLE II

ROLLING-UP TIME CONSTANT AND CORE RADIUS

	Time Constant [s]	Core Radius[m]
B747	2.27	4.67
B757	1.44	2.88

and B757 vortices generated during landing are used for this validation effort, whose circulation taken from [31] and core radius estimated from [32]

$$\rho_c = 0.2\sqrt{\frac{\Gamma_o\, s}{U}} \tag{44}$$

where s is aircraft wing span and U is the landing speed, are listed in Table I. From Eqs. (29) and (44), the rolling-up time constant T and core radius are estimated as shown in Table II. Other parameters adopted in the numerical calculation are air density [3], $\rho_o = 1.2\,\text{kg/m}^3$, the sound speed, $c_o = 340\,\text{m/s}$, longitudinal window size $L_2 - L_1 = 20\,\text{m}$, and the distance between vortex and observation point, $r = 60\,\text{m}\,(\sim 200\,\text{ft})$. The choice of the particular distance represents the nominal aircraft altitude at the middle marker location, which has operational significance from wake turbulence perspectives.

The numerical result of the pressure spectrum for the benchmark (BMK) vortex profile of Eq. (39) is compared against the closed form solution and shown in Fig. 3. Note that good agreement is found, where the Sound Pressure Level (SPL) in decibel scale, $P_r = 20\log_{10}(P/P_o)$, is computed using the Threshold of Hearing (i.e., $P_o = 2\times 10^{-5}\,\text{N/m}^2$) as the reference (see Appendix C). The overall trend in the calculated spectra is similar to the recent phased microphone array measurements of [20] for rolling-up vortices generated during out-of-ground effect. It is further noted that the computed spectra do not suggest

the presence of distinct audible high frequency sound that has sometimes been reported in field observations. A candidate explanation is that since the prescribed vortex is of laminar state in a quiescent environment, mechanisms such as small scale turbulence and their interactions with the vortex which could manifest themselves in higher frequency sound, were not considered. Otherwise stated, the computed spectra is based on the aspect of vortex dynamics that is always present and robust, and can be considered as a baseline spectra. The higher frequency sound sometimes heard when vortices are near the ground is speculated to be caused by the turbulence generated from vortex-ground interactions. This would explain the unpredictable nature in the audible portion of the vortex sound [4].

The good agreement provided the necessary confidence to employ the numerical code with the more realistic vortex models of Eqs. (36) and (37). Characteristics of two specific aircraft types, B747 and B757, are listed in Table I. It is worth noting again from Eq. (39) that the core radius is an important parameter. However, a satisfactory universal scaling scheme for the core size relative to aircraft and atmospheric parameters is still an area of research. Core radii listed in Table I may be over-estimated, but can still be taken as values reflecting the relative sizes of the two example aircraft.

Velocity profile models for the Hallock-Burnham, Lamb-Oseen and the benchmark profile (38) leading to a closed solution of Eq. (39), generated by B747 and B757, are illustrated in Fig. 2. Note that, in all of these profile models, the peak velocities appear at $\rho = \rho_c$. In addition, the peak values are the same in comparison between B747 and B757, owning to the fact that the peak value is proportional to the ratio of Γ_o/ρ_c which is constant in the case presented. Also notice that the benchmark profile has the same peak value as the Hallock-Burnham vortex, but decays more rapidly after $\rho > \rho_c$ than both Hallock-Burnham and Lamb-Oseen vortices. It also shows that the vortex profile for larger aircraft (e.g., B747) spreads out wider than that for smaller aircraft (e.g., B757).

Fig. (3) also shows the numerical results of sound pressures for Hallock-Burnham and Lamb-Oseen vortices generated by B747 and B757, respectively, at the distance of 60 m ($\sim 200\,\mathrm{ft}$). The integration in Eq. (35) is performed by using trapezoidal method. In comparison with vortices with different core sizes, it is found that the vortex with faster
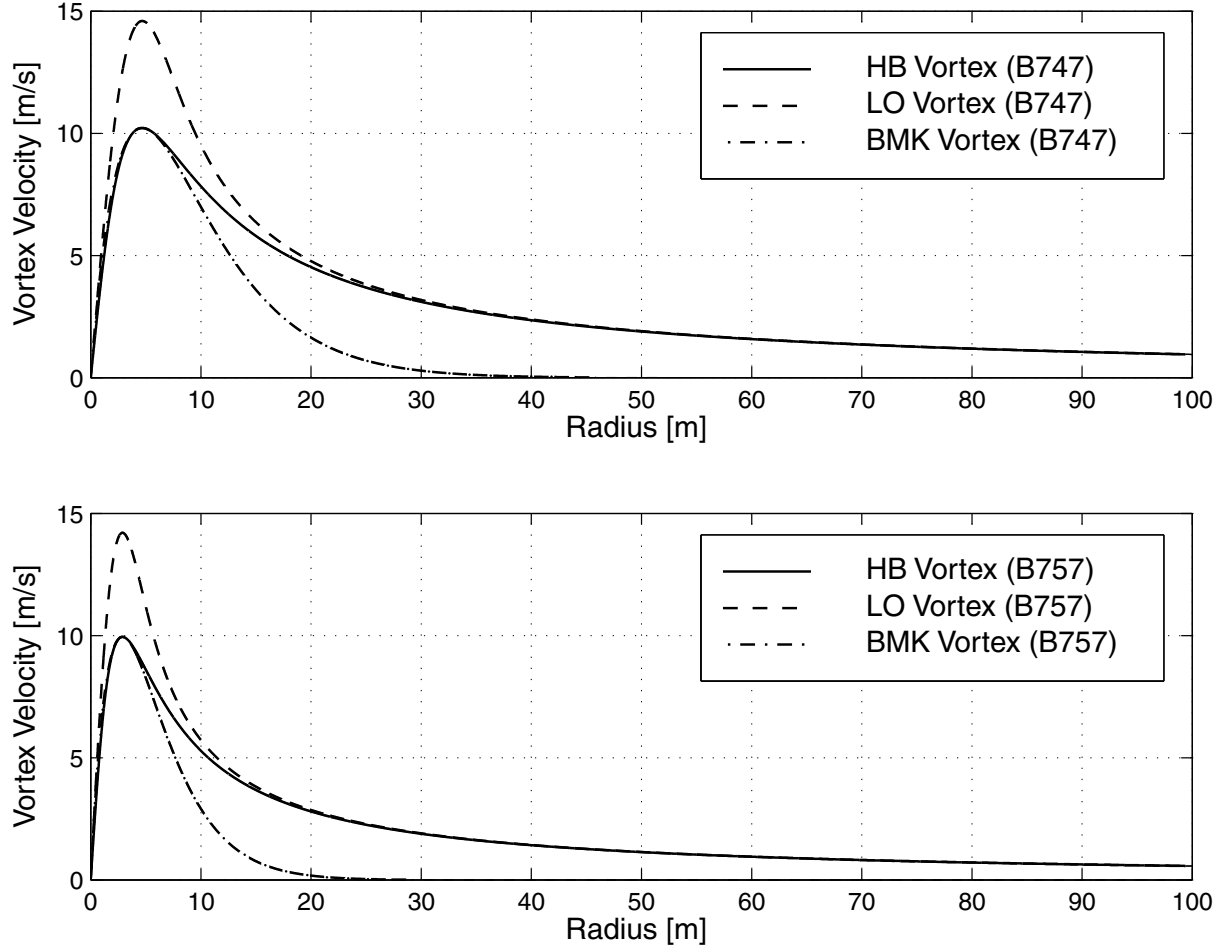
Fig. 2. Velocity profiles for the benchmark (BMK), Hallock-Burnham, and Lamb-Oseen vortices generated by B747 (upper plot, $\Gamma_o = 600\,\mathrm{m^2/s}$, $\rho_c = 4.67\,\mathrm{m}$) and B757 (lower plot, $\Gamma_o = 360\,\mathrm{m^2/s}$, $\rho_c = 2.88\,\mathrm{m}$), respectively.

decaying velocity produces a wider frequency band for its sound pressure. For example, the B757 generates a wider spectrum of vortex sound than the B747 does. On the other hand, as expected, larger aircraft (B747) create higher vortex sound around the peak value.

D. Gain Pattern of Sensor Array

The factor $L_2 - L_1$ in Eqs. (35) and (39) indicates the vortex length from which the sound is detected. Physically, it can be implemented by using a linear phased microphone array deployed under the vortex as illustrated in Fig. 4.
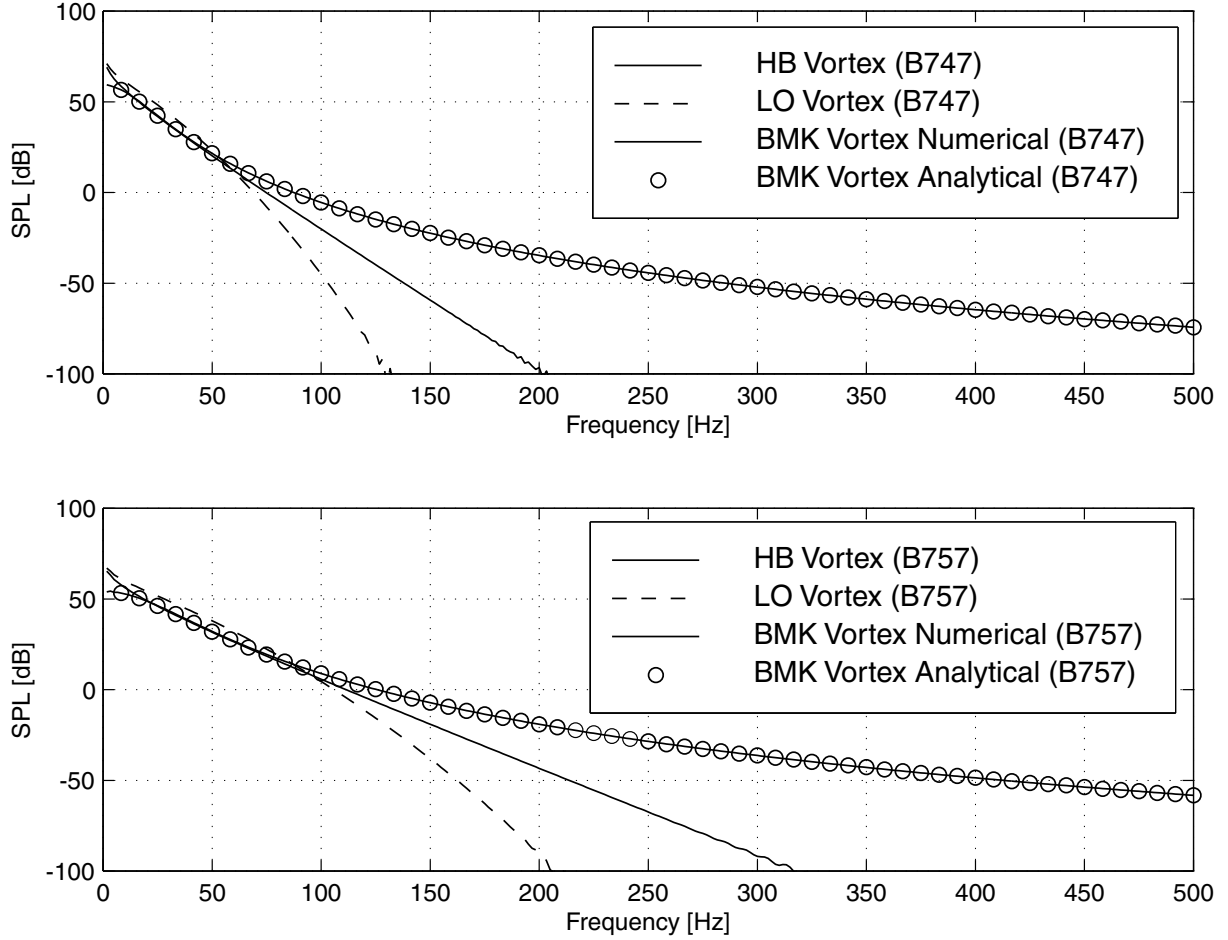
Fig. 3. Spectra of sound pressure for Hallock-Burnham (HB), Lamb-Oseen (LO), and benchmark (BMK) vortices, with constant velocity distribution along flight path, generated by B747 and B757, respectively, at distance $r = 60\,\mathrm{m}\,(\sim 200\,\mathrm{ft})$. For B747, the circulation is $\Gamma_o = 600\,\mathrm{m^2/s}$, and the core radius is $\rho_c = 4.67\,\mathrm{m}$; for B757, the circulation is $\Gamma_o = 360\,\mathrm{m^2/s}$, and the core radius is $\rho_c = 2.88\,\mathrm{m}$.

Denoting the locations of the vortex source and the n-th sensor as z and nd, respectively, the distance between the vortex and the sensor can be expressed as

$$L_n(z) = \sqrt{((z - nd)^2 + r^2)} \tag{45}$$

In addition, by assuming that the total number of sensors in the array is N, the spacing between sensors is d, and the height of the vortex region is r, then the output, which is the coherent sum of the signals from all sensors, is obtained as

$$S(f, z) = \sum_{n=-(N-1)/2}^{n=(N-1)/2} P(f) \exp\left(jkL_n(z)\right) \tag{46}$$
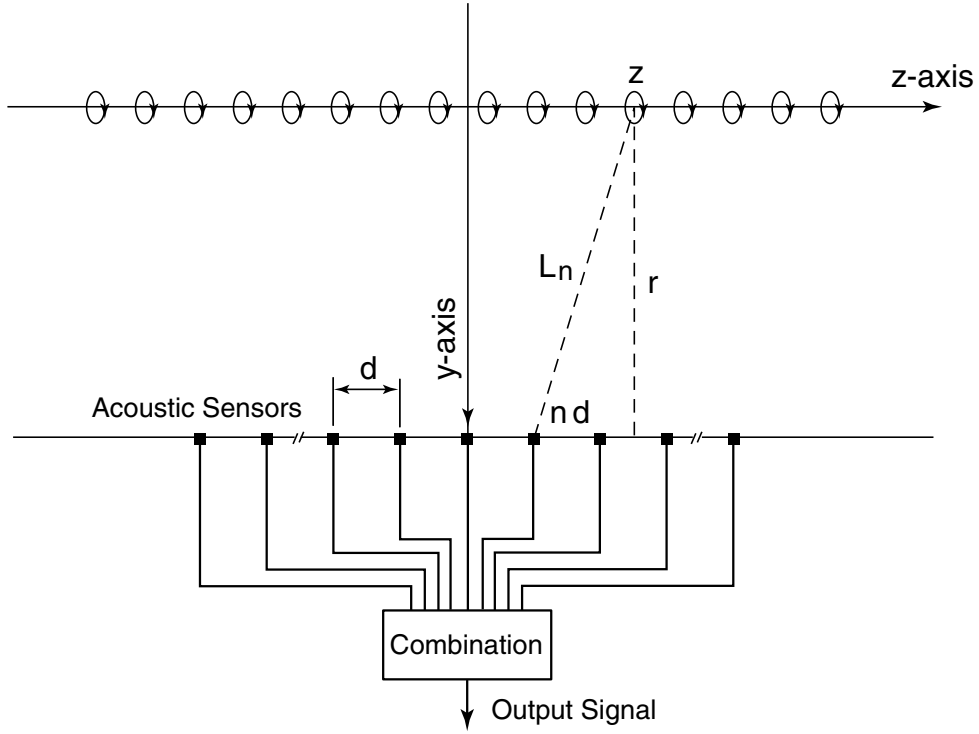
Fig. 4. Layout of acoustic sensor array along aircraft flight path.

where k is the wavenumber, $k = 2\pi f/c_o$, with f and c_o denoting the frequency and speed of sound in free space, respectively, and $P(f)$ is the Fourier transform of the sound signal detected by a single microphone sensor. Finally the normalized gain pattern of the sensor array is calculated by

$$G(f, z) = 20 \log \left(\frac{|S(f, z)|}{|S(f, 0)|} \right) \qquad (47)$$

Fig. (5) shows the numerical result of the gain pattern for the array operated at frequency $f = 50\,\text{Hz}$, where the spacing between elements is $d = 1\,\text{m}$, the number of elements $N = 19$, and the height of the vortex region is $r = 60\,\text{m}$. Note that the region for the gain higher than -3 dB is $-10\,\text{m} \le z \le 10\,\text{m}$, implying that only the vortex in the range of $[-10\,\text{m}, 10\,\text{m}]$ contributes significantly to the output after the combination of signals from the sensor array, as assumed in the numerical simulations for the vortex sound spectrum performed in this report. Another usefulness of using the sensor array is to enhance the power of the sound spectrum. If M arrays are used with each array possessing N elements, the output power of the spectrum will gain approximately $20 \log(MN)$ dB. For
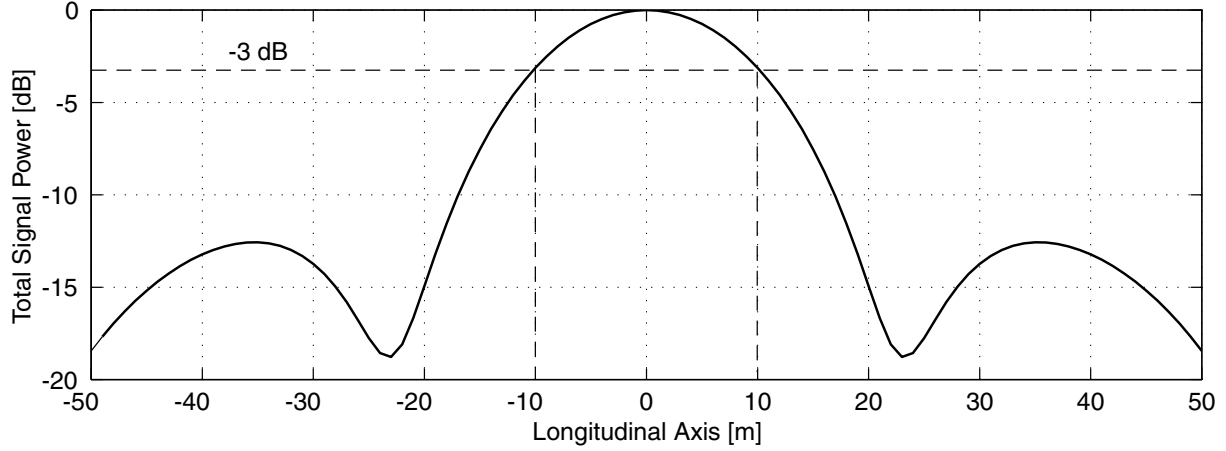
Fig. 5. Gain pattern of acoustic sensor array with $N = 19$ elements along aircraft flight path for vortex sound frequency of $f = 50\,\mathrm{Hz}$. The array spacing is $d = 1\,\mathrm{m}$.

example, if $M = 5$ and $N = 19$, then the gain will be 40 dB.

VI.   Summary and Closing Remarks

The spectral characteristics of sound generated by the rolling-up process of wake vortices at out-of-ground effect altitude have been analytically examined. The acoustic signature was derived from a tensor analysis on the acoustic analogy equation, which ultimately lead to a general analytical expression of the spectra. The influence of the core radius, vortex velocity profile, and circulation are also examined by performing calculations for two representative aircraft, namely, B747 and B757. The vortex sound spectrum was found to be of broadband nature, with a characteristically higher sound level located in region below 100 Hz. The SPL drops off very rapidly after the aforementioned region with increasing frequency. For example, the calculations revealed that at an altitude of 60 m ($\sim 200\,\mathrm{ft}$) away from the vortex, the sound pressure is as high as 60 dB with respect to the Threshold of Hearing, which is equivalent to listening to softly spoken human voice from a distance of 1 ft (0.3m). While for frequency higher than 100 Hz, the sound pressure is lower than the TOH, indicating that it would not be audible in a typically well trafficked airport environment. It is important to note that turbulent flow mechanisms around the cores have not been modeled in this analysis. The computed spectra is therefore representative of the baseline characteristic from a line vortex during

rolling-up. The high energy content situated around the infrasound regime may render itself conductive to wake monitoring, as the atmospheric attenuation effect is less severe. However, it may be more practical from a sensor perspective to monitor frequencies higher than the infrasound regime. Finally, as the speed of sound is relatively slow (compared to light) in reaching a detector which translates to a level of uncertainty in the detected wake locations, the passive acoustic scheme of wake monitoring, if can be proven to perform reliably, is envisioned to be a sensor with a practical range less than a mile.

VII.   Appendices

A.   Derivation of Eq. (22)

The function $F(\bar{r}', \omega)$ in Eq. (19) is the Fourier transform of $f(\bar{r}', t')$, written as

$$
\begin{aligned}
F(\bar{r}', \omega) &= \int f(\bar{r}', t') e^{j\omega t'} dt' \\
&= \nabla' \cdot \nabla' \cdot \int \left[\bar{u}(\bar{r}', t') \bar{u}(\bar{r}', t') \right] e^{j\omega t'} dt'
\end{aligned}
\tag{48}
$$

By using the identity

$$
\phi \nabla' \cdot \bar{a} = \nabla' \cdot (\phi \bar{a}) - \bar{a} \cdot \nabla' \phi
\tag{49}
$$

where $\phi = \dfrac{e^{j\omega|\bar{r}-\bar{r}'|/c_o}}{4\pi |\bar{r} - \bar{r}'|}$ and $\bar{a} = \nabla' \cdot \overline{\overline{A}}(\bar{r}', \omega)$ with the tensor $\overline{\overline{A}}$ expressed explicitly in Eq. (20), and ignoring the surface integral term assuming the vortex disappears at infinite distance [29][1], the spectrum is found as

$$
P(\bar{r}, \omega) = -\rho_o \int \left(\nabla' \cdot \overline{\overline{A}}(\bar{r}', \omega) \right) \cdot \nabla' \phi \, d\bar{r}'
\tag{50}
$$

Furthermore, applying the identity

$$
\left(\nabla' \cdot \overline{\overline{A}} \right) \cdot \bar{b} = \nabla' \cdot \left(\overline{\overline{A}} \cdot \bar{b} \right) - \mathrm{trace} \left(\overline{\overline{A}}^t \cdot \nabla' \bar{b} \right)
\tag{51}
$$

where $\bar{b} = \nabla' \phi$, again ignoring the surface integral and notifying the symmetry property of the tensor, $\overline{\overline{A}} = \overline{\overline{A}}^t$, the compact form of the spectrum is then obtained as shown in Eq. (22).

---

[1]The Divergence Theorm is applicable both for vector and tensor $\mathcal{A}$ with the form $\int \nabla \cdot \mathcal{A} d\bar{r} = \oint d\bar{s} \cdot \mathcal{A}$.

B.   Closed Form Spectrum for Benchmark Vortex

Introducing the velocity profile of the benchmark vortex, Eq. (38), into the integral form of spectrum, Eq. (32), after conducting the integration over ρ', the following expression is obtained,

$$
\begin{aligned}
P(\bar{r}, \omega) &= j \frac{3 \rho_o e^2}{2 c_o^2 \rho_c^4 \pi r}\left(\frac{\Gamma_o}{2 \pi}\right)^2\left(L_2-L_1\right) e^{j \omega r / c_o} \omega \\
&\cdot \int_0^{2 \pi} \frac{\cos ^2 \phi'}{\left(\omega / c_o \sin \phi'+j 2 / \rho_c\right)^4} d \phi'
\end{aligned}
\tag{52}
$$

Note that the integral term has the general form

$$
A(\omega)=\int_0^{2 \pi} \frac{\cos ^2 \phi'}{(a \sin \phi'+j b)^4} d \phi'
\tag{53}
$$

where $a=\omega / c_o$ and $b=2 / \rho_c$. By making change of the variable, $z=e^{j \phi'}$, Eq. (53) becomes a contour integral along a unit circle on the complex plane,

$$
A(\omega)=\frac{4}{j a^4} \oint \frac{z\left(z^2+1\right)^2}{\left(z-\frac{b}{a}+\frac{\sqrt{a^2+b^2}}{a}\right)^4\left(z-\frac{b}{a}-\frac{\sqrt{a^2+b^2}}{a}\right)^4} d z
\tag{54}
$$

where the integrand can be expanded as

$$
\begin{aligned}
\text{Integrand} = &\frac{z\left(z^2+1\right)^2}{\left(\alpha_o-\beta_o\right)^4}\left\{\frac{1}{\left(z-\alpha_o\right)^4}+\frac{1}{\left(z-\beta_o\right)^4}\right. \\
&-4 \frac{1}{\left(\alpha_o-\beta_o\right)} \frac{1}{\left(z-\alpha_o\right)^3}+4 \frac{1}{\left(\alpha_o-\beta_o\right)} \frac{1}{\left(z-\beta_o\right)^3} \\
&+10 \frac{1}{\left(\alpha_o-\beta_o\right)^2} \frac{1}{\left(z-\alpha_o\right)^2}+10 \frac{1}{\left(\alpha_o-\beta_o\right)^2} \frac{1}{\left(z-\beta_o\right)^2} \\
&\left.-20 \frac{1}{\left(\alpha_o-\beta_o\right)^3} \frac{1}{\left(z-\alpha_o\right)}+20 \frac{1}{\left(\alpha_o-\beta_o\right)^3} \frac{1}{\left(z-\beta_o\right)}\right\}
\end{aligned}
\tag{55}
$$

with α_o and β_o expressed, respectively, as,

$$
\alpha_o, \beta_o=\frac{b}{a} \pm \frac{\sqrt{a^2+b^2}}{a}
\tag{56}
$$

Then using the Cauchy's integral formula

$$
f^{(n)}\left(\alpha_o\right)=\frac{n!}{2 \pi j} \oint \frac{f(z)}{\left(z-\alpha_o\right)^{n+1}} d z
\tag{57}
$$

the integration of Eq. (54) is found in a closed form as Eq. (40). Finally the closed form solution of the sound spectrum for the benchmark vortex profile is obtained as Eq. (39).

C.   *Vortex Sound Pressure Level vs. Threshold of Hearing*

The vortex sound, P, is expressed as the Sound Pressure Level (SPL) in decibel scale with respect to the pressure of the Threshold of Hearing (TOH). The intensity of the TOH is $I_o = 10^{-12}\,\text{W/m}^2$ for a single tone at 1 kHz [33], thus the pressure of the TOH is $P_o = 2.0 \times 10^{-5}\,\text{N/m}^2$ according to the relation [25]

$$I_o = \frac{P_o^2}{\rho_o c_o} \tag{58}$$

A 0-dB SPL represents the level of sound pressure at $P = P_o$, and a 74-dB SPL is equivalent to the sound pressure of human normal speech at 1-foot (0.3 m) distance.

VIII.   **Acknowledgment**

REFERENCES

[1] M. J. Lighthill, "On sound generated aerodynamically: I. General theory," *Proceedings of the Royal Society of London, Series A*, vol. 211, pp. 564–587, 1952.

[2] V. J. Rossow, "Lift-generated vortex wakes of subsonic transport aircraft," *Progress in Aerospace Science*, vol. 35, pp. 507–660, 1999.

[3] T. Gerz, F. Holzäpfel, and D. Darracq, "Commercial aircraft wake vortices," *Progress in Aerospace Science*, vol. 38, pp. 181–208, 2002.

[4] J. N. Hallock and W. R. Eberle, "Aircraft wake vortices: A state-of-the-art review of the United States R&D program," FAA-RD-77-23, 1977.

[5] M. Harris, R. I. Young, F. Köpp, A. Dolfi, and J.-P. Cariou, "Wake vortex detection and monitoring," *Aerospace Science Technology*, vol. 6, pp. 325–331, 2002.

[6] D. C. Burnham, "November 1996 Kennedy airport wake vortex test: Sensor evaluation," DOT-VNTSC-FA727-PM-97-27, 1997.

[7] L. J. Garodz and K. L. Clawson, "Vortex wake characteristics of B757-200 and B767-200 aircraft using the tower fly-by technique, Volume 1," NOAA Technical Memorandum ERL ARL-199, Jan. 1993.

[8] D. C. Burnham, "Characteristics of a wake-vortex tracking system based on acoustic refractive scattering," *Journal of the Acoustical Society America*, vol. 61, pp. 647–654, Mar. 1977.

[9] M. Balser, C. A. McNary, and A. E. Nagy, "Acoustic backscatter radar system for tracking aircraft trailing vortices," *Journal of Aircraft*, vol. 11, no. 9, pp. 556–562, Sep. 1974.

[10] L. H. Back, "Optical and physical requirements for fluid particles marking trailing vortices from aircraft," *Journal of Aircraft*, vol. 13, no. 7, pp. 483–489, July 1976.

[11] S. Abramson and D. C. Burnham, "Ground-based anemometer measurements of wake vortices from landing aircraft at airports: Characterisation and modification of wakes from lift," AGARD CP-584, pp. 13.1–13.7, May 1996.

[12] J. N. Hallock, S. P. Ozgood, and J. Konopka, "Wake vortex effects on parallel runway operation," AIAA Paper 2003-0379, 2003.

[13] R. M. Heinrichs and T. J. Dasey, "Analysis of circulation data from a wake vortex lidar," AIAA Paper 1997-0059, 1997.

[14] S. M. Hannon and J. A. Thomson, "Aircraft wake vortex detection and measurement with pulsed solid-state coherent laser lidar," *Journal of Modern Optics*, vol. 41, no. 11, pp. 2175–2196, Nov. 1994.

[15] C. L. Britt, D. P. C. Nguyen, and G. Koch, "Pulsed lidar measurements of aircraft wake vortices at DFW and JFK," AIAA Paper 1999-0982, vol. 463, 1999.

[16] S. Boluriaan and P. J. Morris, "Two-dimensional simulation of wake vortex detection using RASS," 39th AIAA Aerospace Sciences Meeting & Exhibit, Reno, NV, pp. 8–11, Jan. 2001.

[17] J. N. Hallock, "Pressure measurements of wake vortices near the ground," *Journal of Aircraft*, vol. 9, no. 4, pp. 311–312, April 1972.

[18] W. L. Rubin D. C. Burnham E. A. Spitzer and R. P. Rudis, "Robust low cost airport wake vortex sensor," *Journal of Aircraft*, vol. 37, no. 3, pp. 377–382, May-June 2000.

[19] D. C. Burnham and J. N. Hallock, "Chicago monostatic acoustic vortex sensor system," Report No. DOT-TSC-FAA-79-103. IV, p. 206, 1982.

[20] U. Michel and P. Böhning, "Investigation of aircraft wake vortices with phased microphone arrays," AIAA Paper 2002-2501, 2002.

[21] A. Bedard, NOAA, Private Communication, 2002.

[22] A. Powell, "Theory of vortex sound," *Journal of the Acoustical Society America*, vol. 36, no. 1, pp. 177–195, Jan. 1964.

[23] T. Kambe, "Acoustic emissions by vortex motions," *Journal of Fluid Mechanics*, vol. 173, pp. 643–666, 1986.

[24] R. C. K. Leung and N. W. M. Ko, "The interaction of perturbed vortex rings and its sound generation," *Journal of Sound and Vibration*, vol. 202, no. 1, pp. 1–27, 1996.

[25] W. Möhring, "On vortex sound at low mach number," *Journal of Fluid Mechanics*, vol. 85, no. 4, pp. 685–691, 1978.

[26] J. Mathews and R. L. Walker, *Mathematical Methods of Physics*, Addison-Wesley, New York, 2nd ed., 1970.

[27] A. Powell, "Why do vortices generate sound," *Trans. ASME*, vol. 117, pp. 252–260, June 1995.

[28] J. R. Spreiter and A. H. Sacks, "The rolling up of the trailing vortex ¿sheet and its effect on the downwash behind wings," *Jounal of Aeronautic Science*, vol. 18, no. 1, pp. 21–32, Jan. 1951.

[29] J. Van Bladel, *Electromagnetic Fields*, McGraw-Hill, New York, 1964.

[30] M. Abramowitz and I. A. Stegun, *Handbook of Mathematical Functions*, Dover, New York, 1970.

[31] D. Darracq, A. Corjon, F. Ducros, M. Keane, D. Buckton, and M. Redfern, "Simulation of wake vortex detection with airborne doppler lidar," *Journal of Aircraft*, vol. 37, no. 6, Nov.-Dec. 2000.

[32] A. A. Woodfield, "En-route encounters with wake vortices and the implications of reduced vertical separation minima (RVSM)," Woodfield Aviation Research Report No. 9901, 1999.

[33] E. Zwicker and H. Fastl, *Psychoacoustics: Facts and Models*, Springer-Verlag, New York, 2nd ed., 1999.

REPORT DOCUMENTATION PAGE

1. REPORT DATE (DD-MM-YYYY)	2. REPORT TYPE	3. DATES COVERED (From - To)
01- 12 - 2003	Contractor Report	

4. TITLE AND SUBTITLE

Spectral Characteristics of Wake Vortex Sound During Roll-Up

5a. CONTRACT NUMBER

5b. GRANT NUMBER

5c. PROGRAM ELEMENT NUMBER

6. AUTHOR(S)

Zhang, Yan; Wang, Frank Y.; and Hardin, J. C.

5d. PROJECT NUMBER

IAA-1-600

5e. TASK NUMBER

5f. WORK UNIT NUMBER

23-137-30-10

7. PERFORMING ORGANIZATION NAME(S) AND ADDRESS(ES)

NASA Langley Research Center
Hampton, VA 23681-2199

Volpe National Transportation Systems Ctr.
Surveillance and Assessment Division
55 Broadway, Kendall Square
Cambridge, MA 02142

8. PERFORMING ORGANIZATION REPORT NUMBER

9. SPONSORING/MONITORING AGENCY NAME(S) AND ADDRESS(ES)

National Aeronautics and Space Administration
Washington, DC 20546-0001

10. SPONSOR/MONITOR'S ACRONYM(S)

NASA

11. SPONSOR/MONITOR'S REPORT NUMBER(S)

NASA/CR-2003-212673

12. DISTRIBUTION/AVAILABILITY STATEMENT

Unclassified - Unlimited
Subject Category 71
Availability: NASA CASI (301) 621-0390   Distribution: Standard

13. SUPPLEMENTARY NOTES

Zhang and Wang: Volpe National Trans. Systems Center; Hardin: Titan Corp.
An electronic version can be found at http://techreports.larc.nasa.gov/ltrs/ or http://ntrs.nasa.gov
Langley Technical Monitor: Earl R. Booth, Jr.

14. ABSTRACT

This report presents an analysis of the sound spectra generated by a trailing aircraft vortex during its rolling-up process. The study demonstrates that a rolling-up vortex could produce low frequency (less than 100 Hz) sound with very high intensity (60 dB above threshold of human hearing) at a distance of 200 feet from the vortex core. The spectrum then drops off rapidly thereafter. The study suggests that acoustic sensors operating at low frequency band could be profitably deployed for detecting the vortex sound during the rolling-up process.

15. SUBJECT TERMS

Vortex sound; Aircraft wake; Vortex noise

16. SECURITY CLASSIFICATION OF:			17. LIMITATION OF ABSTRACT	18. NUMBER OF PAGES	19a. NAME OF RESPONSIBLE PERSON
a. REPORT	b. ABSTRACT	c. THIS PAGE			STI Help Desk (email: help@sti.nasa.gov)
U	U	U	UU	30	19b. TELEPHONE NUMBER (Include area code) (301) 621-0390